FULL PAPER

Magnetic Resonance in Medicine 000:000–000 (2011)

Arterial Spin Labeling MRI Study of Age and Gender Effects on Brain Perfusion Hemodynamics

Yinan Liu,[1,2]* Xiaoping Zhu,[3] David Feinberg,[4,5] Matthias Guenther,[6,7] Johannes Gregori,[7] Michael W. Weiner,[1,4] and Norbert Schuff[1,4]

Normal aging is associated with diminished brain perfusion measured as cerebral blood flow (CBF), but previously it is difficult to accurately measure various aspects of perfusion hemodynamics including: bolus arrival times and delays through small arterioles, expressed as arterial-arteriole transit time. To study hemodynamics in greater detail, volumetric arterial spin labeling MRI with variable postlabeling delays was used together with a distributed, dual-compartment tracer model. The main goal was to determine how CBF and other perfusion hemodynamics vary with aging. Twenty cognitive normal female and 15 male subjects (age: 23–84 years old) were studied at 4 T. Arterial spin labeling measurements were performed in the posterior cingulate cortex, precuneus, and whole brain gray matter. CBF declined with advancing age ($P < 0.001$). Separately from variations in bolus arrival times, arterial-arteriole transit time increased with advancing age ($P < 0.01$). Finally, women had overall higher CBF values ($P < 0.01$) and shorter arterial-arteriole transit time ($P < 0.01$) than men, regardless of age. The findings imply that CBF and blood transit times are compromised in aging, and these changes together with differences between genders should be taken into account when studying brain perfusion. Magn Reson Med 000:000–000, 2011. © 2011 Wiley Periodicals, Inc.

Key words: arterial spin labeling; arterial-arteriole transit time; age; bolus arrival time; brain perfusion; gender

Many previous studies have shown that age affects brain physiology (1–3), using cerebral blood flow (CBF). CBF reflects the rate of delivery of nutrients to the brain. Furthermore, to characterize the hemodynamics of brain perfusion, a mean transit time for blood circulation based on the central volume principle has also been derived (4,5). However, absolute measurements of blood circulation remain complex, especially in studies of brain aging, because age-related morphological alterations of the brain vasculature, such as increased vessel tortuosity (6–8) potentially altering transit times and dispersion of blood flow tracers, can result in misleading information (9). Accurate measurements of blood circulation are therefore important for an unambiguous interpretation of CBF alterations in the aging brain.

Arterial spin labeling (ASL) MRI, which uses endogenous blood water as tracer for CBF, has excellent prerequisites for studying blood circulation in detail (10–19). Unlike contrast-enhanced MRI, which requires the injection of a "dye" as tracer or positron emission tomography (PET) and single photon computed tomography (20,21), which use radioactive tracers, ASL-MRI can be performed repeatedly, enabling the study of blood circulation at an unprecedented temporal resolution, e.g., by gradually incrementing the postlabeling delay time to sample the evolution of the ASL signal (19). Furthermore, several ASL studies attempted quantifying perfusion hemodynamics of the brain using mathematical models, in which regional variations in transit time of an ASL bolus, inhomogeneous dispersion, and finite exchange rates between tissue compartments were taken into account (22–25). Several ASL studies investigated variations of regional CBF in aging but most did not account for variable transit times of the water labels (15). More recently, further investigations focused on the optimization of ASL parameters to capture variations in transit times more accurately (13). However, most studies relied on bolus arrival time (BAT) alone as proxy for transit delays of the spin labels (11,12,18,26), which may lack sensitivity in capturing subtle alterations of the brain vasculature in aging and dementia, such as increased vessel tortuosity. Recently, we introduced a dual-compartment distributed perfusion model, in which variations in BAT are decomposed into transit delays through large arteries and delays through smaller arteries and arterioles, expressed as arterial-arteriole transit time (aaTT), before the spin labels reach the capillary bed and perfusion into brain tissue. In addition, volumetric ASL acquisition methods that offer sensitive and efficient mapping of brain perfusion simultaneously in three dimensions (17) helped avoid many of the time lag problems in two-dimensional acquisitions (10,13,14,16). In this study, we used the volumetric ASL acquisition together with the distributed perfusion model to investigate in greater detail how brain perfusion hemodynamics vary with advancing age.

[1]Center for Imaging of Neurodegenerative Diseases, Department of Veterans Affairs Medical Center, San Francisco, California, USA.

[2]Northern California Institute for Research and Education, San Francisco, California, USA.

[3]Wolfson Molecular Imaging Centre, University of Manchester, United Kingdom.

[4]Department of Radiology and Biomedical Imaging, University of California, San Francisco, USA.

[5]Advanced MRI Technology LLC, Sebastopol, California, USA.

[6]Mediri GmbH, Heidelberg, Germany.

[7]Fraunhofer MEVIS, Bremen, Germany.

Grant sponsor: National Center for Research Resources (NCRR); Grant number: P41 RR 023953; Grant sponsor: VA Medical Center, San Francisco; Grant number: 01EV0702, sponsored by the German Ministry of Education and Research (BMBF).

*Correspondence to: Yinan Liu, Ph.D., Center for Imaging of Neurodegenerative Diseases, Department of Veterans Affairs Medical Center, 4150 Clement Street, San Francisco, CA 94121. E-mail: yinan.liu@va.gov

Received 13 June 2011; revised 30 September 2011; accepted 13 October 2011.

DOI 10.1002/mrm.23286
Published online in Wiley Online Library (wileyonlinelibrary.com).

Our primary goals were 2-fold. First, we aimed to replicate previous findings of regional reductions in CBF with advancing age by taking into account variations in bolus transit times, including BAT and aaTT. Second, we sought to determine the extent to which each transit time component changes characteristically with advancing age. On the basis of the previous reports of gender differences in hemodynamics (12,14,27), we also explored the extent to which transit delays differ between women and men. Finally, to determine the benefit of modeling aaTT, we tested the accuracy to predict age based on various parameters of brain hemodynamics.

MATERIALS AND METHODS

Subjects

Thirty-five cognitive normal subjects, who participated in various imaging studies of normal human brain and cognitive decline at our MRI center and who had dynamic ASL-MRI scans were selected for this study. The group consisted of 20 female and 15 male subjects, who were equally distributed across the age range from 23 to 84 years (mean age ± SD: 52.7 ± 18.7 years; median age 58 years). At least three subjects were represented in each decade of age, with the exception of the eighth decade, which included one subject only. To exclude cognitive impairment, the subjects received a battery of neurocognitive tests, including the mini-mental state exam for assessments of global cognitive functioning (28), and the CVLT II immediate and delayed recall trials for assessment of memory functions (29). None of the subjects had a clinical history of a psychiatric illness, epilepsy, diabetes, major heart disease, primary and secondary hypertension, head trauma, or alcoholism. In addition, a neuroradiologist visually inspected the MRI data for any incidental pathology (none detected) and scored the severity of white matter lesions (WMLs, not an exclusion criterion) in both periventricular and deep white matter regions on a four-level scale, following the Fazekas criteria (30). Finally, the apolipoprotein E (APOE) genotype was determined for each subject to control for the genetic polymorphism related to the risk for developing dementia. A summary of the demographic, neurocognitive, and genetic data is provided in Table 1. The study protocol was approved by the Committees of Human Research at the University of California in San Francisco and the VA Medical Center in San Francisco, and each subject gave signed informed consent before participating in the study.

Table 1
Demographics and Clinical Characteristics of the Study Population

	Male	Female	*P*-value
Number of participants	15	20	
Age range (years)	26–76	23–84	0.2
Age mean ± SD (years)	47.8 ± 19.9	56.4 ± 18.8	0.6
Mini-mental state exam[a]	29.3 ± 1.1	29.5 ± 0.9	0.6
Memory[b]			
Immediate recall	15.9 ± 3.3	16.7 ± 4.3	0.7
Delayed recall	14.1 ± 3.7	14.5 ± 4.4	0.6
APOE [2/3; 3/3;3/4;4/4][c]	3:9:3:0	3:13:3:1	0.7
WML severity[d]	0.6 ± 1.0	1.3 ± 1.6	0.2

[a]Mini-mental state exam; scores range from 0 to 30 with higher values indicating less cognitive impairment.
[b]Memory tests based on California Verbal Learning Test battery: score range from 0 to 60 with higher scored indicating more impairment.
[c]Apolipoprotein E gene alleles; the frequency of each allele is listed; note, 2/2 and 2/4 were not present in this study population.
[d]White matter lesions based on a 0–4 rating scale following the Fazekas criteria.

MRI Acquisition

Imaging was performed on a 4T MRI system (Bruker Biospec, Germany), equipped with a single housing birdcage transmit and an eight-channel phased-array receive head coil. MRI included: (1) volumetric T_1-weighted magnetization-prepared rapid acquisition gradient echo images with repetition time/echo time/inversion time [TI] = 2300/3.37/950 msec, flip angle = 7°, $1 \times 1 \times 1$ mm^3 resolution. Magnetization-prepared rapid acquisition gradient echo images were used for tissue segmentation and as anatomical reference. (2) Volumetric (three-dimensional, 3D) T_2-weighted images based on a variable flip angle turbo spin-echo sequence with repetition time/echo time = 3000/356 ms, a train of 109 echoes and $1 \times 1 \times 1$ mm^3 in-plane resolution. T_2-weighted images were used as intermediates in registering ASL-MRI to magnetization-prepared rapid acquisition gradient echo images. (3) Pulsed ASL-MRI, using the FAIR labeling scheme (31) and 3D mapping of the ASL signal using gradient- and spin-echo imaging (17), consisting of a single 460 ms echo train for signal readout with 5/8 Fourier phase encoding and $64 \times 33 \times 20$ matrix size. The 3D gradient- and spin-echo images were further zero-filled, yielding a nominal resolution of $2.5 \times 2.5 \times 4$ mm^3. For dynamic ASL measurements, a series of 13 image frames were acquired with variable postlabeling delay times TI = 0, 0.2, 0.5, 0.8, 1.0, 1.2, 1.4, 1.6, 1.8, 2.0, 2.2, 2.4, and 2.6 s. Repetition time/echo time were 3000/23.3 ms, respectively. The acquisition time for each postlabeling delay frame was 24 s. A total of 13 postlabeling frames were acquired and each frame was averaged four times before the next postlabeling delay increment. The acquisition of an entire ASL series took about 6 min.

ASL Model of Perfusion Dynamic

We briefly outline the model for the parameterization of perfusion dynamic based on the evolution of the ASL signal. Full details of the model can be found in Ref. 24. The essential features of the model are sketched in Fig. 1b. The model has two key features: First, the evolution of the ASL signal is decomposed into four phases with respect to the propagation of the labels through the cerebral vasculature and second, the spatial distribution of the labels is compartmented with considerations of a finite transfer rate for water crossing the blood brain barrier and a stepwise process toward a homogeneous water distribution in each compartment. The decomposition of the signal evolution into multiple phases has the

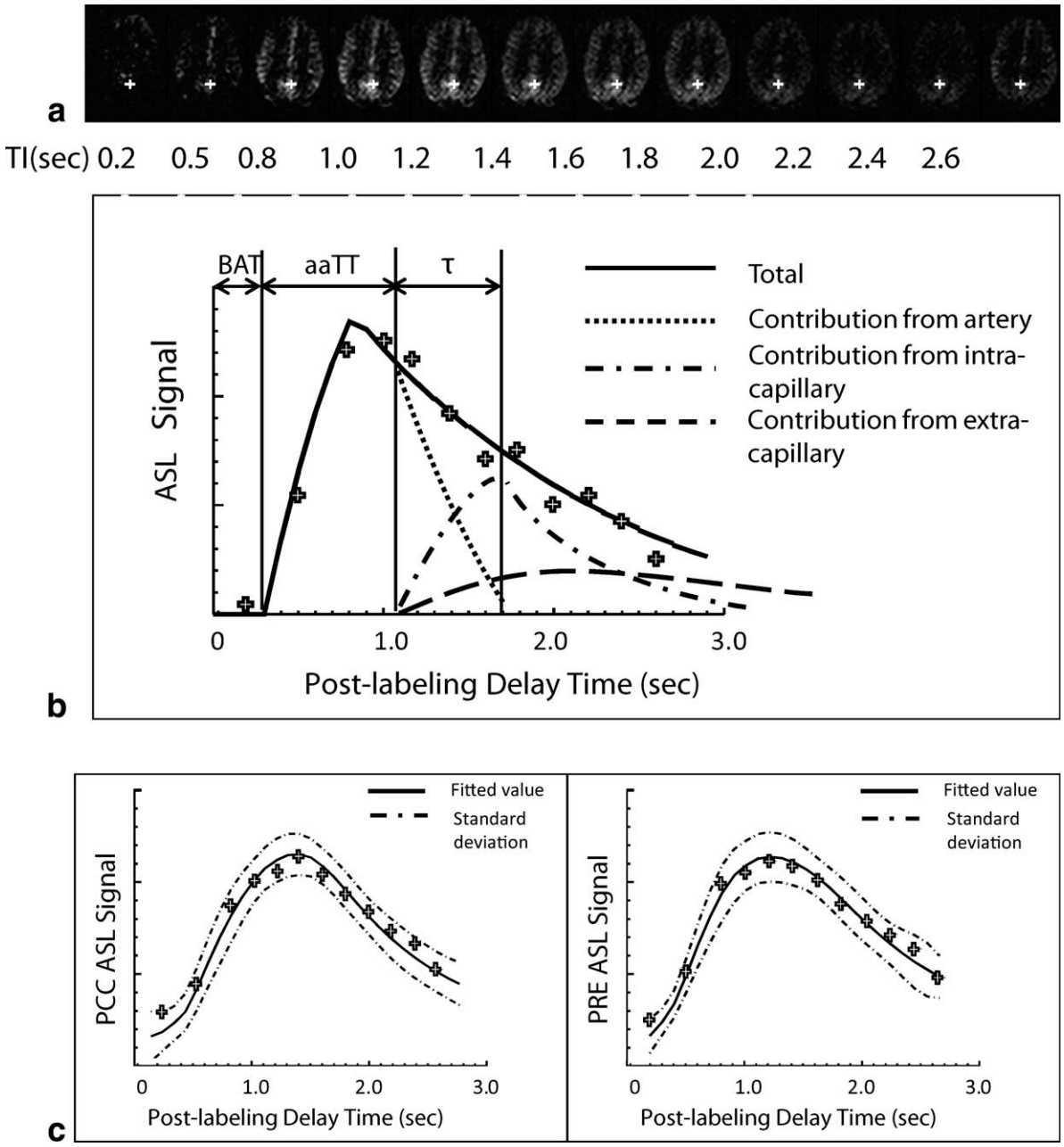

FIG. 1. **a**: Representative perfusion weighted images of an ASL-MRI series with variable postlabeling delay times (TI) from a 65-year-old subject. The white cross in the images indicates the location of the posterior cingulated cortex, a region of particular interest in this study. **b**: Experimental ASL data from the posterior cingulate cortex region (the white cross) showing the time course of the ASL signal as a function of postlabeling delay time and overlaid the corresponding fit (solid line) and the decomposition of the signal into arterial, intracapillary, and extracapillary components, according to the four-phase perfusion model.24 The timing parameters of the model, as used in this study, including bolus arrival time (BAT), arterial-arteriole transit time (aaTT), and bolus duration (τ) are also indicated. **c**: The average ASL signal and fitted curve in PCC and PRE together with the standard deviation of the fitting errors.

advantage that various transit periods, which are related to the different physical processes of the bolus propagation, can be taken into account. Specifically, the four phases of the ASL time course include: (1) the transit phase, termed BAT, in which the labeled blood water travels from the labeling plane until it reaches the voxel of interest; (2) the arterial phase, termed aaTT, during which the labeled blood water transits through arteries and arterioles before water exchange starts; (3) the arterial-capillary transitional phase, which is defined by the bolus duration (τ), during which only a fraction of the labeled blood water has entered the capillary bed for exchange; and (4) the capillary phase, in which all of the labeled blood water has entered the capillary bed for exchange. The magnitude of the ASL signal during each phase is diminished by longitudinal spin relaxation. In this study, exchange rate and spin relaxation were fixed.

Parameter Estimations of Dynamic ASL

We used the simplex minimization procedure to model the ASL signal (32). Discrete values were estimated for CBF, BAT, aaTT, and tau, while fixed values were used for the permeability surface-area product (PS = 340 mL blood/100 mL tissue/min (33)), tissue T_1 relaxation (1723 ms), and blood T_1 relaxation (1914 ms (34)) across voxels and subjects to reduce the degrees of freedom of the model and to stabilize the fits. Computations were performed voxel-by-voxel in Matlab (The MathWorks, Natick, MA), and results summarized as 3D parametric maps of CBF, BAT, and aaTT, as well as a map of residual standard fitting errors. To quantify absolute value of CBF in physiological units of ml blood/100 ml tissue/min, the equilibrium magnetization of blood was approximated as the mean CSF value of the first unlabeled and hence fully relaxed proton density weighted image (echo time = 23.2 ms) of the ASL series (35).

Image Segmentation and Region of Interest Selection

The ASL data were evaluated selectively for perfusion of gray matter (GM) and for specific brain structures known for diminished functions with advancing age, such as the posterior cingulate cortex (PCC) and the precuneus (PRE) (36,37). PCC and PRE were chosen because as they are part of default mode brain network and were previous demonstrated significant distinguish between Alzheimer's disease and healthy aging (36,38,39). To achieve anatomical correspondence between structural and ASL-MRI data, first the 3D untagged ASL image sets were coregistered to the corresponding T_2-weighted images using affine transformations, followed by registering the T_2-weighted images to the corresponding high-resolution T_1-weighted images using high-dimensional warping algorithm in SPM2 (Statistical Parametric Mapping; the Wellcome Trust Center for Neuroimaging, UK) that provided the transformation parameters to ultimately register ASL-MRI to the T_1-weighted images. Furthermore, the T_1-weighted images were segmented into GM, white matter (WM), and cerebrospinal fluid (CSF) based on tissue probabilistic distributions using SPM2. A GM mask was generated (i.e., for voxels containing more than 80% GM) to extract selectively ASL data of GM. A threshold of 80% for GM has been used as cutoff in many previous studies (40–42), and we also selected this level based on our empirical experience with partial volume effect in ASL. The threshold did not result in significant differences in voxel numbers for ASL between young/old or male/female subjects. In addition, the brain atlas from the Montreal Neurological Institute (http://packages.bic.mni.mcgill.ca/tgz/) was used to extract ASL data selectively from PCC and PRE by reslicing and coregistering the Montreal Neurological Institute atlas to the ASL untagged images in the individual space of each subject. The mean values of CBF, BAT, and aaTT within each region of interest (global GM, PCC, and PRE) were then calculated based on the corresponding parametric ASL maps. The remaining analysis focuses on regional perfusion dynamics in global GM, PCC, and PRE.

Statistics

Linear regression was used to model relationships between the various parameterized ASL measures as dependent variables and age, gender, and age by gender interactions as factors. To determine the contribution of individual factors to the model, multiple models were constructed with and without inclusion of the specific factors and compared pairwise using *F*-tests. We accounted initially for severity of WMLs and APOE genotype in the model, because direct effects of these factors on CBF variations were previously reported (43,44) but found no significant contributions from these factors. We therefore ignored WMLs and APOE genotype as factors in the rest of the analysis to reduce the risk of overfitting. The significance of regional differences between PCC and PRE in age-related CBF and transit time variations were determined by comparing the coefficient distributions from the corresponding regressions, supplemented by bootstrap and Wilcoxon tests (45,46).

To determine accuracy of age predictions based on various parameters of brain hemodynamics, we used the functional form of a relevance vector machine, a machine learning algorithm based on sparse Bayesian generalized linear modeling (47). The error between predicted and true age was then used as metric for ranking the predictive power of each ASL measure. Relevance vector machine was chosen, because the algorithm provides first parsimonious solutions for regressions and second generates probabilistic instead of discrete predictions. The procedure was augmented by bootstrapping, yielding distributions of errors from each ASL measure that allowed determining the significance in ranking the measures. Differences in accuracy were tested pairwise using *t*-tests with a threshold of $\alpha = 0.05$ for significance.

RESULTS

The summary of demographic and clinical data in Table 1 indicates that there were no significant differences between women and men in age range, cognitive status, severity of WMLs, and APOE genotype. A representative set of ASL data from a 65 years old subject is shown in Fig. 1a. The time course of the ASL signal from one voxel in the PCC region is shown in Fig. 1b with the corresponding four-phase decomposition superimposed. The average ASL signal and fitted curve in PCC and PRE are shown in Fig. 1c together with the standard deviation of the fitting error. The corresponding parametric maps of CBF, BAT, and aaTT as well as a map of the root mean square fitting errors before the data were masked by 80% GM are shown in Fig. 2.

Aging and Gender Effects

Estimations of age and gender effects on the various measures of perfusion dynamic are summarized in Table 2, separately for each parameter, i.e., CBF, BAT, and aaTT as well as by regions of interest. The regression coefficients and standard errors are listed, representing baseline value (i.e., intercept), change per decade of age and the difference between the genders of each perfusion

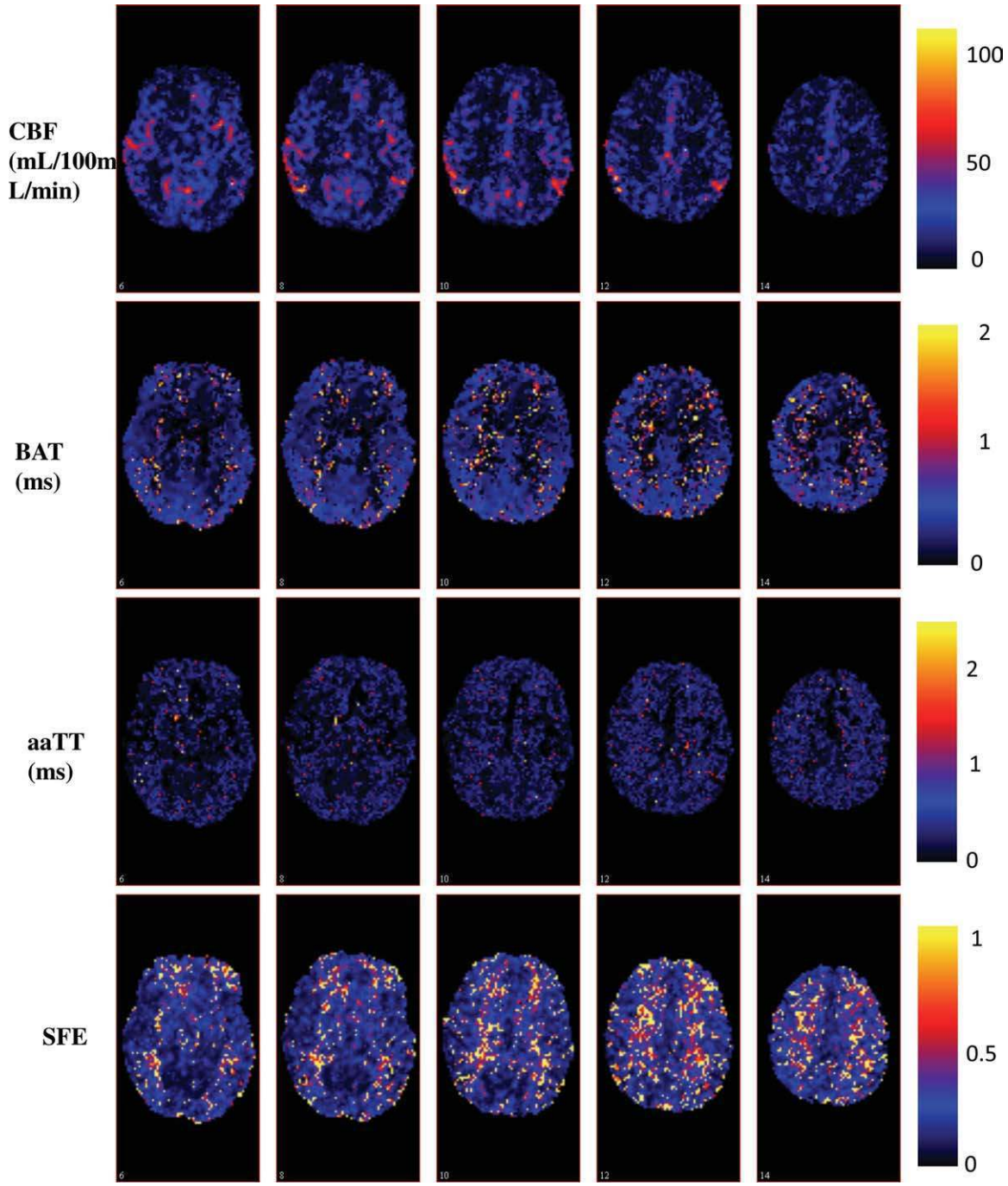

FIG. 2. Representative parametric maps of cerebral blood flow (CBF), bolus arrival time (BAT), arterial-arteriole transit time (aaTT), and standardized fitting errors from a 65-year-old subject. Parameter maps were obtained based on the four-phase perfusion model.

measure in physical units. The statistical significance of variations is also listed. With respect to aging, CBF of global GM declined by about 7.7% per decade of age from the CBF intercept value of 48 mL/100 mL/min compared with 7.8% decline per decade for PCC and 8.8% decline per decade for PRE. aaTT of global GM increased by about 2.1% per decade of age from the intercept value of 0.38 s compared with 8.0% increase per decade for PCC while aaTT of the PRE did not change significantly. BAT increased in all three regions significantly between 12 and 21% per decade of age from the intercept value of 0.26 s. Accounting for severity of WMLs as well as for APOE genotype did not significantly alter the effects of age on the values of perfusion dynamic.

With respect to gender, we found significant differences across the perfusion measures and regions but no significant interactions between advancing age and gender, implying gender effects are independent of age. Specifically, women had generally higher CBF values than men by about 11.7% for global GM, by 14.9% for the PCC, and by 13.9% for the PRE, relative to the respective intercept values (listed in Table 2). Woman had shorter

Table 2
Age and Gender Effects on the Perfusion Measures by Brain Regions

Variables/regions	Intercept	Age	Sex	$\|t_{age}\|$	$\|t_{sex}\|$
Units	mL/100 mL/min	mL/100 mL/min/decade	mL/100 mL/min Men versus women		
CBF					
GM	47.67 ± 2.95	−3.6 ± 0.5	−5.62 ± 1.86	7.18***	3.02**
PCC	62.41 ± 5.31	−4.9 ± 0.9	−9.29 ± 3.35	5.64***	2.78**
PRE	41.69 ± 4.44	−3.7 ± 0.7	−5.78 ± 2.80	5.11***	2.07*
Units	Seconds	Seconds/decade	Seconds Men versus women		
aaTT					
GM	0.38 ± 0.02	0.01 ± 0.00	0.05 ± 0.01	2.25*	3.31**
PCC	0.25 ± 0.05	0.02 ± 0.01	0.06 ± 0.03	2.60*	1.63
PRE	0.27 ± 0.03	0.01 ± 0.00	0.06 ± 0.02	1.50	2.67*
BAT					
GM	0.26 ± 0.04	0.03 ± 0.007	0.09 ± 0.03	4.60***	3.7**
PCC	0.24 ± 0.09	0.05 ± 0.02	0.08 ± 0.06	3.6**	1.3
PRE	0.22 ± 0.05	0.03 ± 0.007	0.11 ± 0.03	4.20***	3.4**

Listed are the coefficients of the linear regressions ± standard errors.
$|t_{age}|$ and $|t_{sex}|$ indicate the *t*-scores of the factors age and sex in the linear regressions; Significance code: <0.001 "***"; 0.001 "**"; 0.01 "*"; 0.05 "•"; 0.1 " ".
GM: gray matter; PCC: posterior cingulate cortex; PRE: precuneus; CBF: cerebral blood flow; aaTT: arterial-arteriole transit time; BAT: bolus arrival time.

BAT values than men, ranging from 33 to 50% of the respective intercept values. Finally, women also had shorter aaTT values than men by 12.1% for global GM, by 22.4% for the PCC, and by 21.1% for the PRE. ANOVA tests showed that variations in CBF were generally more dependent on age than gender (CBF: $F = 10.1$, $P = 0.003$). Similar results were obtained for aaTT and BAT.

The regression plots shown in Figs. 3 and 4 illustrate the effects of age and gender on the measures of perfusion dynamic (i.e., CBF, BAT, and aaTT), separately for global GM (Fig. 3), the PCC, and the PRE (Fig. 4).

Regional Variations

Differences in perfusion parameters between PCC and PRE were also significant. At baseline, the PCC had 33% higher CBF values than the PRE ($P < 0.05$). The age decline in CBF was 11.5% less for the PCC than for the PRE ($P < 0.05$). On the other hand, PCC and PRE had similar BAT values at baseline, while the increase in BAT with age was 34.5% higher for PCC than for PRE ($P < 0.05$). Finally, PCC and PRE had similar aaTT values at baseline but the increase in aaTT with age was 62.9% higher for PCC than for PRE ($P < 0.05$).

Accuracy of Age Prediction

Distributions of errors in predicting age based on the various perfusion measures are shown in Figure 5. The results show CBF yielded the smallest prediction error, indicating it has the most predictive power for age, followed by aaTT. BAT yielded the largest prediction error. Differences between the measures in predicting age were all significant at the $p < 0.0001$ level.

DISCUSSION

We have three major findings: First, we found significant reduction of CBF in the posterior cingulate, precuneus, and global GM region with advancing age, consistent with many other aging studies of brain perfusion using various imaging techniques, including PET and single photon computed tomography. Importantly, the influence of age on CBF remained significant even after accounting for variations in bolus transit delays. The results establish more firmly than before that CBF is diminished due to aging even after accounting for major confounding effects from vascular alterations. Second, a new finding is the prolongation in aaTT with advancing age, globally in GM as well as regionally in the posterior cingulate cortex. Moreover, measurements of the aaTT improved predictions of age-related decline in blood volume compared with measurements based on BAT alone. The prominent role of aaTT in predicting perfusion changes related to aging is consistent with histological findings of systematic morphological changes in arterioles with advanced aging, such as increased tortuosity (6–8), which would increase path length and thus prolong transit time. Third, we found gender—in addition to aging—also affected perfusion with women presenting overall higher CBF values and shorter aaTT than men, although age had overall a stronger effect on perfusion than gender. Taken together, the findings suggest that CBF, as well as bolus transits are compromised with advancing age and the age effect together with differences between genders should be taken into account when studying brain perfusion.

Our finding of CBF reductions with advancing age are consistent with many other imaging studies, using a variety of measurements techniques, including PET, single photon computed tomography (2,20,21,48), and ASL-MRI (14,15). Still, some studies reported no significant

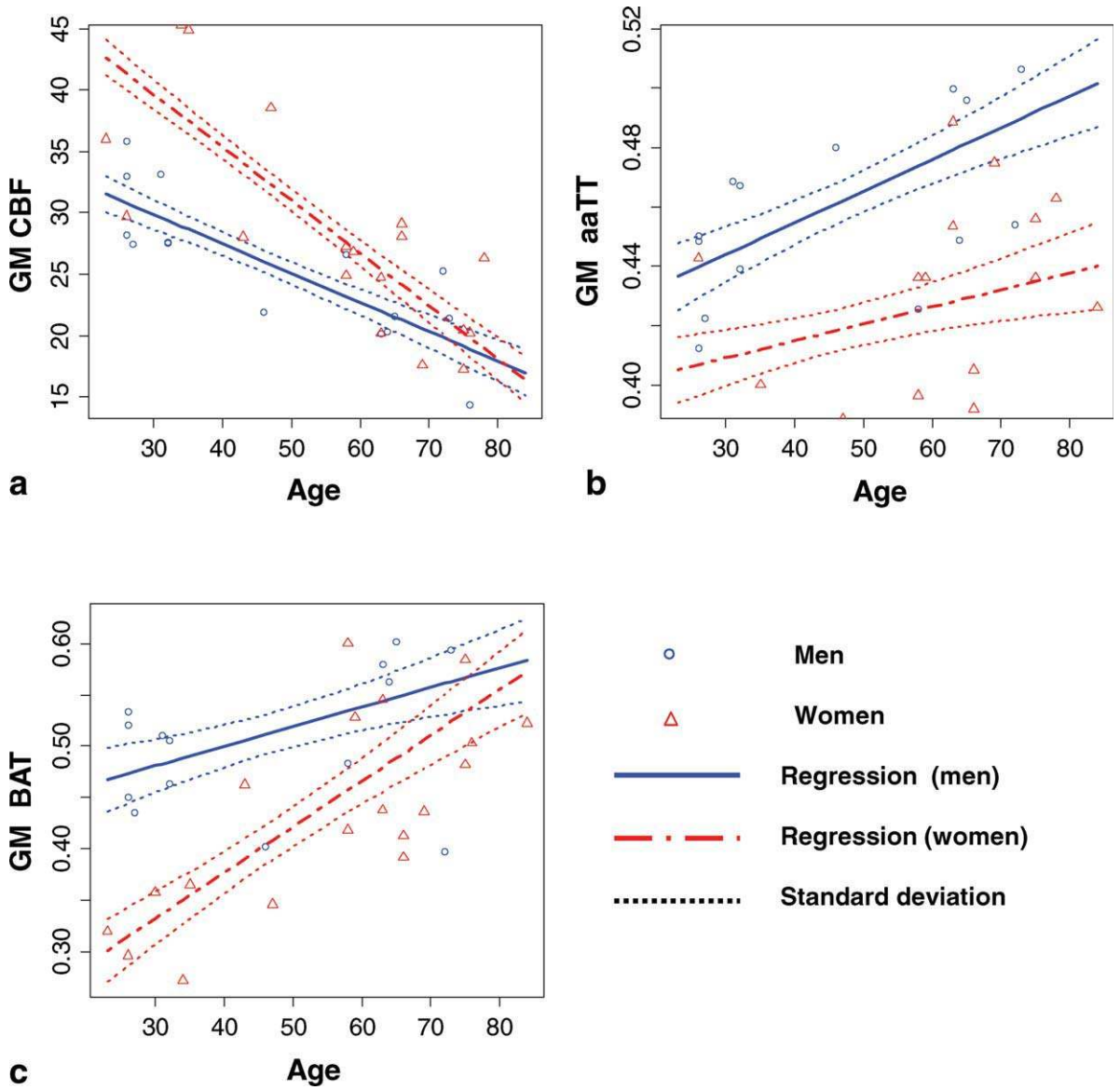

FIG. 3. Scatter plots of perfusion dynamic variables for global gray matter (GM) versus age, separately for women (triangle) and men (circle). Parameter estimates of perfusion based on linear regressions (men:solid line; women:dot-dash line)are indicated in the plots together with the corresponding standardized fitting errors (dotted lines). Plots show separately results for a) cerebral blood flow (CBF), b) arterial-arteriole transit time (aaTT), and c) bolus arrival time (BAT).

correlations between CBF and aging (49,50). Interestingly, the rate of CBF decline with aging in our study is similar in magnitude to rates reported by O^{15}-PET studies (2). In particular, the relatively high rate in CBF decline of the posterior cingulate compared with the decline of the precuneus and global GM is also consistent with previous reports using PET (48), although other studies found even high rates of CBF decline with aging in other brain regions, such as the anterior cingulate (51). It is noteworthy that most PET and single photon computed tomography studies did not account for partial volume effects and some studies reported that the aging-related CBF reductions disappeared after partial volume corrections (50). In contrast, we still found significant CBF reductions after limiting the analysis to predominantly GM regions to circumvent partial volume problems. The result implies that the CBF reduction cannot simply be interpreted as an artifact of structural alterations in the aging brain. In absence of major structural confounds, our findings could potentially help to better understand the energy metabolism of the aging brain (7).

A new finding is the prolongation in aaTT with advancing age, indicating that variations in blood circulation can accompany aging. In particular, the finding that the prediction of age improved with information from aaTT is intriguing and suggests that the decomposition of the postlabeling delay into aaTT provides potentially useful information for aging which cannot be discerned from BAT alone. Similarly, ASL techniques designed to eliminate or compensate for transit effects

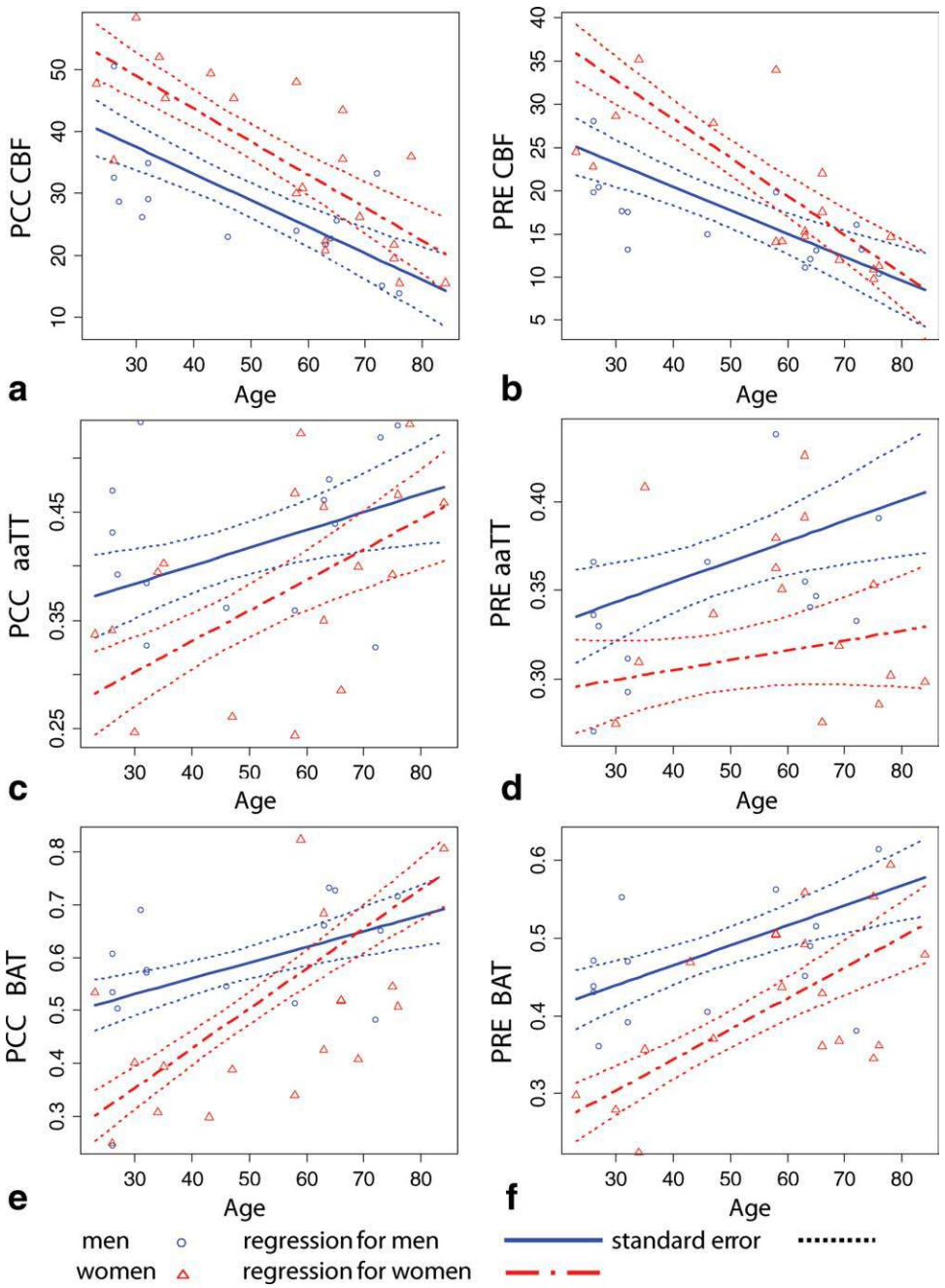

FIG. 4. Scatter plots of regional perfusion dynamic variables versus age, for posterior cingulated cortex (PCC) and precuneus (PRE), separately for women (triangle) and men (circle), similar to the plots shown in Figure 3.

might miss important information about the microvascular change, which causes variation in transit time and blood circulation due to aging or dementia (52,53). Recently, another ASL study also reported variations in transit time due to through large and small vessels, implying that a decomposition of the transit time benefits the characterization of brain perfusion (10). Our finding that aaTT plays an important role in predicting perfusion changes related to aging is consistent with histological findings of systematic morphological changes in arteries and arterioles with advancing age that includes increased vessel tortuosity, including large carotid vessels and arterioles (7,8). Arterioles, which are typically less than 100 μm in diameter and thus markedly smaller than even small arteries (400 μm) but still larger than capillaries (54,55), present usually the greatest resistance to blood flow (56) and also complete the change from pulsatile to steady flow when blood enters the capillaries (57). In addition to increased tortuosity of arterioles, histological studies also found increased rarefaction (58) and increased damage of arteriole walls, potentially prolonging the transit time of blood as well (6–8). Our findings of an increased aaTT might therefore reflect compromised structure and morphology of brain vasculature with aging, impacting cerebral blood supply.

An interesting and unexpected observation is that aaTT of the PCC increased markedly with advancing age compared with the one of PRE, despite similar aaTT baseline values of both brain structures at young age.

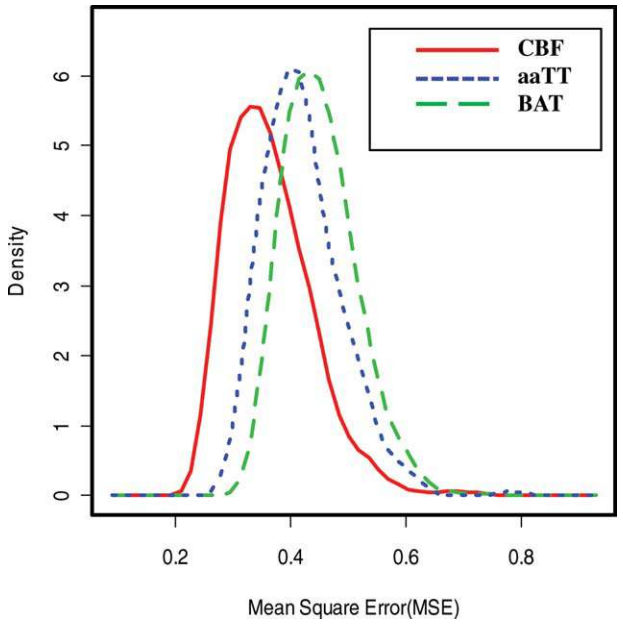

FIG. 5. Accuracy of various perfusion dynamic parameters in predicting aging using relevance vector machine algorithm. Density plots of the distribution of mean square errors (MSE) from predictions of age based on the various perfusion variables, i.e., cerebral blood flow (CBF), bolus arrival time (BAT) and arterial-arteriole transit time (aaTT), are shown using a relevance vector machine algorithm. A small MSE value indicates a more accurate prediction.

The PCC and PRE are among the highest perfused brain regions and also belong to the socalled default functional brain network (37,59), but both regions are also targets of high deposition of amyloid β-peptide (Aβ), the main component of amyloid plaques in the brain associated with Alzheimer's disease (36,60). Whether the difference in aaTT between the PCC and PRE is also an indication of differences in Aβ pathology remains to be determined.

The third finding of higher CBF values in women than men is consistent with several other perfusion studies using various imaging techniques (27,61) including ASL (14,62). In contrast, the finding of gender differences in aaTT has not been reported before. The reasons for the gender difference in CBF are unclear but possible explanations include variations in the hematocrit (63,64). Woman have lower hematocrit than men, and this could result in increased CBF for two reasons: First, reduced oxygen carrying capacity (due to reduced hematocrit) could result in higher CBF to supply the brain with needed oxygen. Second, reduced hematocrit is associated with reduced blood viscosity which would be consistent with our finding of shorter aaTT values in women, irrespective of age. Shorter aaTT values in women than men are also consistent with observations of gender differences in blood flow velocity and vessel diameter (65,66). More studies are warranted to better understand the biological underpinning of gender differences in brain hemodynamics.

Finally, using differences in error distributions to predict age, we found that CBF ranked highest in terms of accuracy and BAT lowest. We interpret this result as an indication that CBF is more susceptible to aging effects than bolus transit delays. Importantly, aaTT ranked significantly higher than BAT in terms of accuracy despite the fact that BAT is easier to estimate computationally than aaTT. The result implies that the inclusion of aaTT in the model improved the characterization of hemodynamic perfusion. On the other hand, BAT might be more influenced by the experimental design than aaTT, because major contributions to BAT come from large vessels with turbulent blood flow over long distances, causing variable bolus dispersions. The four-phase model (24), providing an estimation of aaTT, is therefore preferable over simpler models especially for studies in which a distinction between perfusion in large and small vessels is important.

Several limitations of our study ought to be mentioned: Our sample size is relatively small for an aging study, and therefore, generalization of our results should be done with caution. Moreover, we assumed CBF and aging are linearly related, which may be a substantial simplification. Furthermore, we did not collect CSF biomarkers of AD, such as $A\beta_{1\text{-}42}$ or tau proteins to exclude the possibility that some of the elders in this population had preclinical AD (67). Hence, some variations in perfusion dynamic could be due to neurodegeneration and not aging. Another complication is that we did not directly control for biological confounds of CBF variations, such as hypertension, diabetes, and caffeine intake at the time of study, although we excluded subjects with a clinical history of hypertension and diabetes. It is therefore possible that some variations in CBF measures are not related to age but induced by peripheral conditions. Another limitation is that we kept the permeability surface (PS) parameter fixed (an index of blood brain barrier permeability) and did not account for variations across subjects, although PS is thought to increase with aging (for a review see: (68)) but difficult to measure reliably using ASL-MRI (69). We also did not determine age-related variations in the apparent T_1 relaxation of the ASL signal due to prohibitively long scan times, although recent MRI studies imply a monotone T_1 increase of GM tissue with older age (70). T_1 of blood serum, on the other hand, seems to be more stable across the life span (71). As effects on the ASL signal from increased blood brain barrier permeability and increased T_1 of GM together can compensate each other, the impact of these variations on estimations of aaTT and CBF are difficult to predict. Our findings should therefore be interpreted with caution in absence of blood brain barrier and brain T_1 measurements. Finally, partial gray and white matter volume may have mimicked reductions in perfusion, despite our restriction to measuring perfusion only in voxels with at least 80% GM.

In summary, our findings suggest that age and to some extend also gender influence not only CBF but also induce variations in blood transit times and thus all aspects of perfusion dynamic need to be considered when interpreting CBF decline in aging.

REFERENCES

1. Celsis P. Age-related cognitive decline, mild cognitive impairment or preclinical Alzheimer's disease? Ann Med 2000;32:6–14.
2. Leenders KL, Perani D, Lammertsma AA, Heather JD, Buckingham P, Jones T, Healy MJ, Gibbs JM, Wise RJ, Hatazawa J, Herold S, Beaney RP, Brooks DJ, Spinks T, Rhodes C, Frackowiak RSJ. Cerebral blood

flow, blood volume and oxygen utilization. Normal values and effect of age. Brain 1990;113 (Pt1):27–47.
3. Marchal G, Rioux P, Petit-Taboue MC, Sette G, Travere JM, Le Poec C, Courtheoux P, Derlon JM, Baron JC. Regional cerebral oxygen consumption, blood flow, and blood volume in healthy human aging. Arch Neurol 1992;49:1013–1020.
4. Ibaraki M, Ito H, Shimosegawa E, Toyoshima H, Ishigame K, Takahashi K, Kanno I, Miura S. Cerebral vascular mean transit time in healthy humans: a comparative study with PET and dynamic susceptibility contrast-enhanced MRI. J Cereb Blood Flow Metab 2007;27:404–413.
5. Calamante F, Thomas DL, Pell GS, Wiersma J, Turner R. Measuring cerebral blood flow using magnetic resonance imaging techniques. J Cereb Blood Flow Metab 1999;19:701–735.
6. Sonntag WE, Lynch CD, Cooney PT, Hutchins PM. Decreases in cerebral microvasculature with age are associated with the decline in growth hormone and insulin-like growth factor 1. Endocrinology 1997;138:3515–3520.
7. Farkas E, Luiten PG. Cerebral microvascular pathology in aging and Alzheimer's disease. Prog Neurobiol 2001;64:575–611.
8. Hutchins PM, Lynch CD, Cooney PT, Curseen KA. The microcirculation in experimental hypertension and aging. Cardiovasc Res 1996; 32:772–780.
9. Calamante F, Gadian DG, Connelly A. Quantification of perfusion using bolus tracking magnetic resonance imaging in stroke. Stroke 2002;33:1146–1151.
10. Chen Y, Wang D, Detre J. Comparison of arterial transit times estimated using arterial spin labeling. Magn Reson Mater Phys Biol Med 2011:1–10.
11. Wang J, Licht DJ. Pediatric perfusion MR imaging using arterial spin labeling. Neuroimaging Clin N Am 2006;16:149–167, ix.
12. MacIntosh BJ, Filippini N, Chappell MA, Woolrich MW, Mackay CE, Jezzard P. Assessment of arterial arrival times derived from multiple inversion time pulsed arterial spin labeling MRI. Magn Reson Med 2010;63:641–647.
13. Campbell AM, Beaulieu C. Pulsed arterial spin labeling parameter optimization for an elderly population. J Magn Reson Imaging 2006; 23:398–403.
14. Parkes LM, Rashid W, Chard DT, Tofts PS. Normal cerebral perfusion measurements using arterial spin labeling: reproducibility, stability, and age and gender effects. Magn Reson Med 2004;51:736–743.
15. Biagi L, Abbruzzese A, Bianchi MC, Alsop DC, Del Guerra A, Tosetti M. Age dependence of cerebral perfusion assessed by magnetic resonance continuous arterial spin labeling. J Magn Reson Imaging 2007; 25:696–702.
16. Dai W, Lopez OL, Carmichael OT, Becker JT, Kuller LH, Gach HM. Mild cognitive impairment and alzheimer disease: patterns of altered cerebral blood flow at MR imaging. Radiology 2009;250:856–866.
17. Gunther M, Oshio K, Feinberg DA. Single-shot 3D imaging techniques improve arterial spin labeling perfusion measurements. Magn Reson Med 2005;54:491–498.
18. Yang Y, Engelien W, Xu S, Gu H, Silbersweig DA, Stern E. Transit time, trailing time, and cerebral blood flow during brain activation: measurement using multislice, pulsed spin-labeling perfusion imaging. Magn Reson Med 2000;44:680–685.
19. Wang J, Alsop DC, Song HK, Maldjian JA, Tang K, Salvucci AE, Detre JA. Arterial transit time imaging with flow encoding arterial spin tagging (FEAST). Magn Reson Med 2003;50:599–607.
20. Krausz Y, Bonne O, Gorfine M, Karger H, Lerer B, Chisin R. Age-related changes in brain perfusion of normal subjects detected by 99mTc-HMPAO SPECT. Neuroradiology 1998;40:428–434.
21. Pagani M, Salmaso D, Jonsson C, Hatherly R, Jacobsson H, Larsson SA, Wagner A. Regional cerebral blood flow as assessed by principal component analysis and (99m)Tc-HMPAO SPET in healthy subjects at rest: normal distribution and effect of age and gender. Eur J Nucl Med Mol Imaging 2002;29:67–75.
22. Chappell MA, MacIntosh BJ, Donahue MJ, Gunther M, Jezzard P, Woolrich MW. Separation of macrovascular signal in multi-inversion time arterial spin labelling MRI. Magn Reson Med 2010;63:1357–1365.
23. St Lawrence KS, Frank JA, McLaughlin AC. Effect of restricted water exchange on cerebral blood flow values calculated with arterial spin tagging: a theoretical investigation. Magn Reson Med 2000;44:440–449.
24. Li KL, Zhu X, Hylton N, Jahng GH, Weiner MW, Schuff N. Four-phase single-capillary stepwise model for kinetics in arterial spin labeling MRI. Magn Reson Med 2005;53:511–518.
25. Parkes LM, Tofts PS. Improved accuracy of human cerebral blood perfusion measurements using arterial spin labeling: accounting for capillary water permeability. Magn Reson Med 2002;48:27–41.
26. Yoshiura T, Hiwatashi A, Yamashita K, Ohyagi Y, Monji A, Takayama Y, Nagao E, Kamano H, Noguchi T, Honda H. Simultaneous measurement of arterial transit time, arterial blood volume, and cerebral blood flow using arterial spin-labeling in patients with Alzheimer disease. AJNR Am J Neuroradiol 2009;30: 1388–1393.
27. Gur RE, Gur RC. Gender differences in regional cerebral blood flow. Schizophr Bull 1990;16:247–254.
28. Folstein MF, Folstein SE, McHugh PR. "Mini-mental state". A practical method for grading the cognitive state of patients for the clinician. J Psychiatr Res 1975;12:189–198.
29. Delis DC, Kramer JH, Kaplan E, Ober BA. California Verbal Learning Test-II. San Antonio, TX: The Psychological Corporation; 2000.
30. Fazekas F, Chawluk JB, Alavi A, Hurtig HI, Zimmerman RA. MR signal abnormalities at 1.5 T in Alzheimer's dementia and normal aging. AJR Am J Roentgenol 1987;149:351–356.
31. Kim SG, Tsekos NV, Ashe J. Multi-slice perfusion-based functional MRI using the FAIR technique: comparison of CBF and BOLD effects. NMR Biomed 1997;10:191–196.
32. FH Walters LP, SL Morgan. Sequential simplex optimization. Florida: CRC Press Boca Raton; 1991.
33. Keiding S, Sorensen M, Bender D, Munk OL, Ott P, Vilstrup H. Brain metabolism of ^{13}N-ammonia during acute hepatic encephalopathy in cirrhosis measured by positron emission tomography. Hepatology 2006;43:42–50.
34. Rooney WD, Johnson G, Li X, Cohen ER, Kim SG, Ugurbil K, Springer CS, Jr. Magnetic field and tissue dependencies of human brain longitudinal 1H2O relaxation in vivo. Magn Reson Med 2007; 57:308–318.
35. Chalela JA, Alsop DC, Gonzalez-Atavales JB, Maldjian JA, Kasner SE, Detre JA. Magnetic resonance perfusion imaging in acute ischemic stroke using continuous arterial spin labeling. Stroke 2000;31: 680–687.
36. Jagust W, Gitcho A, Sun F, Kuczynski B, Mungas D, Haan M. Brain imaging evidence of preclinical Alzheimer's disease in normal aging. Ann Neurol 2006;59:673–681.
37. Pfefferbaum A, Chanraud S, Pitel AL, Muller-Oehring E, Shankaranarayanan A, Alsop DC, Rohlfing T, Sullivan EV. Cerebral blood flow in posterior cortical nodes of the default mode network decreases with task engagement but remains higher than in most brain regions. Cereb Cortex 2011;21:233–244.
38. Minoshima S, Giordani B, Berent S, Frey KA, Foster NL, Kuhl DE. Metabolic reduction in the posterior cingulate cortex in very early Alzheimer's disease. Ann Neurol 1997;42:85–94.
39. Greicius MD, Srivastava G, Reiss AL, Menon V. Default-mode network activity distinguishes Alzheimer's disease from healthy aging: evidence from functional MRI. Proc Natl Acad Sci USA 2004;101: 4637–4642.
40. de Boer R, Vrooman HA, van der Lijn F, Vernooij MW, Ikram MA, van der Lugt A, Breteler MM, Niessen WJ. White matter lesion extension to automatic brain tissue segmentation on MRI. Neuroimage 2009;45:1151–1161.
41. Brickman AM, Zahra A, Muraskin J, Steffener J, Holland CM, Habeck C, Borogovac A, Ramos MA, Brown TR, Asllani I, Stern Y. Reduction in cerebral blood flow in areas appearing as white matter hyperintensities on magnetic resonance imaging. Psychiatry Res 2009;172: 117–120.
42. Altaye M, Holland SK, Wilke M, Gaser C. Infant brain probability templates for MRI segmentation and normalization. Neuroimage 2008;43:721–730.
43. Hogh P, Knudsen GM, Kjaer KH, Jorgensen OS, Paulson OB, Waldemar G. Single photon emission computed tomography and apolipoprotein E in Alzheimer's disease: impact of the epsilon4 allele on regional cerebral blood flow. J Geriatr Psychiatry Neurol 2001;14: 42–51.
44. Schuff N, Matsumoto S, Kmiecik J, Studholme C, Du A, Ezekiel F, Miller BL, Kramer JH, Jagust WJ, Chui HC, Weiner MW. Cerebral blood flow in ischemic vascular dementia and Alzheimer's disease, measured by arterial spin-labeling magnetic resonance imaging. Alzheimers Dement 2009;5:454–462.
45. Hollander M, Wolfe DA. Nonparametric Statistical Methods. New York: Wiley; 1999.
46. Davison AC, Hinkley DV. Bootstrap Methods and their Application. Cambridge: University Press; 1997.

47. Tipping ME. Sparse Bayesian learning and the relevance vector machine. J Machine Learn Res 2001;1:211–244.
48. Martin AJ, Friston KJ, Colebatch JG, Frackowiak RS. Decreases in regional cerebral blood flow with normal aging. J Cereb Blood Flow Metab 1991;11:684–689.
49. Ito H, Kanno I, Ibaraki M, Hatazawa J. Effect of aging on cerebral vascular response to Paco2 changes in humans as measured by positron emission tomography. J Cereb Blood Flow Metab 2002;22:997–1003.
50. Meltzer CC, Cantwell MN, Greer PJ, Ben-Eliezer D, Smith G, Frank G, Kaye WH, Houck PR, Price JC. Does cerebral blood flow decline in healthy aging? A PET study with partial-volume correction. J Nucl Med 2000;41:1842–1848.
51. Schultz SK, O'Leary DS, Boles Ponto LL, Watkins GL, Hichwa RD, Andreasen NC. Age-related changes in regional cerebral blood flow among young to mid-life adults. Neuroreport 1999;10:2493–2496.
52. Alsop DC, Detre JA. Reduced transit-time sensitivity in noninvasive magnetic resonance imaging of human cerebral blood flow. J Cereb Blood Flow Metab 1996;16:1236–1249.
53. Ye FQ, Mattay VS, Jezzard P, Frank JA, Weinberger DR, McLaughlin AC. Correction for vascular artifacts in cerebral blood flow values measured by using arterial spin tagging techniques. Magn Reson Med 1997;37:226–235.
54. Christensen KL, Mulvany MJ. Location of resistance arteries. J Vasc Res 2001;38:1–12.
55. O'Rourke MF, Hashimoto J. Mechanical factors in arterial aging: a clinical perspective. J Am Coll Cardiol 2007;50:1–13.
56. Safar ME, Blacher J, Pannier B, Guerin AP, Marchais SJ, Guyonvarc'h PM, London GM. Central pulse pressure and mortality in end-stage renal disease. Hypertension 2002;39:735–738.
57. Ottesen JT, Olufsen MS, Larsen JK. Applied Mathematical Models in Human Physiology. SIAM: Society for Industrial and Applied Mathematics; 2004.
58. Riddle DR, Sonntag WE, Lichtenwalner RJ. Microvascular plasticity in aging. Ageing Res Rev 2003;2:149–168.
59. Raichle ME, Snyder AZ. A default mode of brain function: a brief history of an evolving idea. Neuroimage 2007;37:1083–1090; discussion 1097–1089.
60. Klunk WE, Engler H, Nordberg A, Wang Y, Blomqvist G, Holt DP, Bergstrom M, Savitcheva I, Huang GF, Estrada S, Ausen B, Debnath ML, Barletta J, Price JC, Sandell J, Lopresti BJ, Wall A, Koivisto P, Antoni G, Mathis CA, Langstrom B. Imaging brain amyloid in Alzheimer's disease with Pittsburgh Compound-B. Ann Neurol 2004;55:306–319.
61. Pirson AS, Vander Borght T, Van Laere K. Age and gender effects on normal regional cerebral blood flow. AJNR Am J Neuroradiol 2006;27:1161–1162; author reply 1162–1163.
62. Alsop DC, Detre JA. Multisection cerebral blood flow MR imaging with continuous arterial spin labeling. Radiology 1998;208:410–416.
63. Baenziger O, Jaggi JL, Mueller AC, Morales CG, Lipp HP, Lipp AE, Duc G, Bucher HU. Cerebral blood flow in preterm infants affected by sex, mechanical ventilation, and intrauterine growth. Pediatr Neurol 1994;11:319–324.
64. Zeng SM, Yankowitz J, Widness JA, Strauss RG. Etiology of differences in hematocrit between males and females: sequence-based polymorphisms in erythropoietin and its receptor. J Gend Specif Med 2001;4:35–40.
65. Jacobs AK, Kelsey SF, Brooks MM, Faxon DP, Chaitman BR, Bittner V, Mock MB, Weiner BH, Dean L, Winston C, Drew L, Sopko G. Better outcome for women compared with men undergoing coronary revascularization: a report from the bypass angioplasty revascularization investigation (BARI). Circulation 1998;98:1279–1285.
66. Muller HR, Brunholzl C, Radu EW, Buser M. Sex and side differences of cerebral arterial caliber. Neuroradiology 1991;33:212–216.
67. Shaw LM, Vanderstichele H, Knapik-Czajka M, Clark CM, Aisen PS, Petersen RC, Blennow K, Soares H, Simon A, Lewczuk P, Dean R, Siemers E, Potter W, Lee VM, Trojanowski JQ. Cerebrospinal fluid biomarker signature in Alzheimer's disease neuroimaging initiative subjects. Ann Neurol 2009;65:403–413.
68. Farrall AJ, Wardlaw JM. Blood-brain barrier: ageing and microvascular disease—systematic review and meta-analysis. Neurobiol Aging 2009;30:337–352.
69. Carr JP, Buckley DL, Tessier J, Parker GJ. What levels of precision are achievable for quantification of perfusion and capillary permeability surface area product using ASL? Magn Reson Med 2007;58:281–289.
70. Westlye LT, Walhovd KB, Dale AM, Bjornerud A, Due-Tonnessen P, Engvig A, Grydeland H, Tamnes CK, Ostby Y, Fjell AM. Differentiating maturational and aging-related changes of the cerebral cortex by use of thickness and signal intensity. Neuroimage 2010;52:172–185.
71. Kariakina NF, Papish EA, Temkina T. Magnetic resonance characteristics of the blood serum of healthy persons. Med Radiol (Mosk) 1988;33:50–52.